International Journal of Fatigue 164 (2022) 107134

Contents lists available at ScienceDirect

International Journal of Fatigue

journal homepage: www.elsevier.com/locate/ijfatigue

Fatigue testing and end of life investigation of a topology optimized connecting rod fabricated via selective laser melting

Silvia Cecchel [a,*], Nima Razavi [c], Francesco Mega [a], Giovanna Cornacchia [b], Andrea Avanzini [b], Davide Battini [b], Filippo Berto [c]

[a] Streparava SpA, Via Zocco 13, 25030 Adro BS, Italy
[b] Department of Mechanical and Industrial Engineering, University of Brescia, via Branze 38, 25123 Brescia, Italy
[c] Department of Mechanical and Industrial Engineering, Norwegian University of Science and Technology (NTNU), Trondheim, Nor4way

ARTICLE INFO

Keywords:
Titanium alloys
Fatigue
Automotive component
Additive manufacturing
Microstructure
Testing

ABSTRACT

A first assessment of product durability of an SLM Ti6Al4V conrod with a lightweighted structure was developed. Full-scale fatigue testing and finite element analyses of testing conditions were performed to determine stress cycles in critical regions. End of life (EOL) and metallurgical analysis completed the study. A fatigue diagram covering the finite life and estimating the infinite life load levels, difficult to estimate a priori, was obtained; this is the first relevant result toward fatigue assessment of AM components. Fatigue life for the SLM conrod was lower than the conventional one, however, EOL analysis pointed out potential future improvements.

1. Introduction

The general advantage of AM [1] is that it allows for the design and development of products having a highly complex shape which are often not feasible with traditional manufacturing technologies. This feature could be of great interest in the automotive field, where the design of a near net shape part could reduce the weight, and thus the vehicle emissions [2–4], while maintaining the same level of mechanical resistance. For engine parts, the benefits resulting from weight reduction are maximized [5–7], since smaller engines are more efficient. The introduction of new technologies in the automotive field, especially for such critical parts, always require a series of validation analyses that reproduce the actual operating conditions, starting from laboratory investigations up to field test. However, to ensure the feasibility of replacing the traditional and consolidated manufacturing methods for serial production in the automotive field, the knowledge about this new emerging technology behaviour needs to be implemented.

This study is part of a wider investigation on the weight reduction of a critical engine component for the automotive field. The development of this product, a connecting rod (conrod), and the related previous studies are briefly introduced below.

Conrod is an intermediate member between the piston and the crankshaft. Its primary function is to transmit the push and pull from the piston pin to the crankpin and thus convert the reciprocating motion of the piston into the rotary motion of the crank. The usual form of the connecting rod in internal combustion engines consists of a long shank, having rectangular, circular, tubular or I/H cross section[8], and a small end and a big end. The small end of the conrod is usually made in the form of an eye and is provided with a bush. The big end is usually split in two halves, so that it can be mounted easily on the crankpin bearing shells. The split cap is fastened to the big end with cap bolts.

A conrod is essentially subjected to alternating direct compressive and tensile forces due to the force acting on the piston as gas pressure and inertia of the reciprocating parts. Compressive forces are much higher than the tensile forces. Other loads include forces due to inertia of the connecting rod (inertia bending and tension forces) and forces generated by friction between contacting elements (i.e. piston rings, piston pin bearing and crankpin bearing). Thus, the most relevant requirement is the achievement of the proper mechanical resistance under loading with a minimum weight to reduce the inertia forces [9]. Quite obviously, connecting rods are subjected to cyclic loading and are typically designed for infinite-life assuming endurance limit as design criterion.

The connecting rods are usually manufactured by steel forging; recently, also titanium alloys are applied for some niche applications to reduce the weight [9–11].

In a previous research study, an innovative approach based on topological optimization of the component under investigation was

* Corresponding author.
E-mail address: s.cecchel@streparava.com (S. Cecchel).

https://doi.org/10.1016/j.ijfatigue.2022.107134
Received 20 December 2021; Received in revised form 30 May 2022; Accepted 11 July 2022
Available online 14 July 2022
0142-1123/© 2022 Elsevier Ltd. All rights reserved.

presented, in order to explore the possibility of using Selective Laser Melting (SLM) in substitution of the most conventional manufacturing processes [12]. The foreseen application field belongs to sectors where high performance is required (i.e. motorbikes and cars for sport competitions); here the weight reduction is a very sensible parameter and the limited production volumes are compatible with this new technology. The design developed can be summarized as an SLM multi-branch structure that allows a weight reduction of 45% and 15% in comparison with steel and titanium forging respectively. Adequate mechanical resistance of this brand-new configuration was foreseen by means of Finite Element Analysis (FEA) analysis. Other benefits related to the new AM design include the manufacturing of the conrod into two separated parts, that avoid some difficult machining operations, and the integration of conformed cooling channels. In order to take full advantage of these potential benefits, a careful work is necessary to properly consider all the aspects connected with the product development: from knowledge of material properties as a function of heat treatments, to investigations on the durability of this new component.

From a material point of view, a Ti6Al4V alloy was selected and a specific experimental activity was performed during a previous work [13] to identify the best heat treatment condition for AM components. The target requirements to be achieved were set as a combination of high mechanical properties (i.e. Yield Strength $\sigma_y = 880$ MPa, Stress at break $\sigma_m = 950$ MPa, Elongation percentage A%=11%), good resistance to corrosion and negligible residual stresses. In particular, three different types of heat treatment on Ti6Al4V were developed and microstructure, mechanical resistance, residual stresses and corrosion resistance were deeply investigated. At the end of this research work a super-β transus solubilization followed by a tempering was found to be the best option to heat treat the SLM conrod [12].

Concerning durability aspects, the fatigue behaviour of conventionally manufactured conrods has been extensively studied in the past (see e.g. [14]), both at component and material specimen level. For additively manufactured alloys, most of the current literature on fatigue only deals with tests on small sized standardized specimens, whereas investigations on real components are actually limited to a few aerospace parts [15]. In particular, focusing on the fatigue behaviour of SLM Ti alloys, data concerning fatigue life in regimes from Low Cycle Fatigue (LCF) to Very High Cycle Fatigue (VHCF) are reported in [16–20]. In recent investigations, the influence of surface post-treatments [21,22,23], built orientation [24,25,26], and scale and thickness effect [27,28,29] were considered, as well as notch sensitivity [30,31,32] and fatigue crack growth aspects [33,34].

Overall, as summarized in [35], fatigue of AM metals usually initiates from defects deriving from the AM process and the fatigue life is usually reduced when comparing as-built AM metals to their wrought counterparts. While post-processing can give AM metals similar fatigue life as wrought materials, the fatigue behaviour of additively manufactured metal alloys remains a wide-open field of research. Indeed, it has been reported that up to 100 different process parameters can affect the fatigue life of AM [36], and also for Ti-6Al-4 V there is an elevate scatter in the fatigue literature data, depending on the process parameters of each individual build [37]. In this scenario, the design of critical structural components utilizing such manufacturing processes is particularly challenging and still in its early stages [38].

Therefore, the present research work is aimed at a first assessment of product durability by full-scale fatigue testing of a Ti6Al4V conrod produced with SLM under loading conditions representative of operating service. Together with fatigue testing, a FEM model of test conditions was implemented to analyse stress cycles in critical regions, which could be useful for the development of fatigue life prediction models. This aspect is particularly relevant when considering the non-conventional structure of the conrod which also provides a unique opportunity to gain insight on fatigue behaviour in complex shaped components generated by topological optimization. The work was integrated with the end of life analysis and detailed metallurgical investigation to complete the information about the component properties and correlate them with the fatigue behaviour of full-scale component.

Overall, this study helps building and consolidating the know-how regarding the SLM technology applied to automotive components and a Design for Additive Manufacturing activity.

2. Materials and methods

2.1. Sample description

The components tested during the present research are SLM multi-branches conrods developed after a topological optimization activity as described in the introduction and in a previous work [12]. They were produced with Ti6Al4V commercial powder from EOS GmbH on a DMLS machine "EOSINT M290" and printed along the direction of the main component axis. One of these parts is presented in Fig. 1. The heat treatment condition is super-β transus solubilization at 1015 °C for 0.5 h followed by tempering at 730 °C for 2 h. The parts were blasted with spherical ceramic beads (diameter 125 – 250 μm) and a maximum pressure of 3 bars, to achieve suitable surface roughness and to remove any oxides formed after SLM production from the surface. The main relevant dimensions of the component are visible in Fig. 1. Into the final assembly, pin holes are bushed. The experimental mechanical properties measured [12] are $\sigma_y = 900 \pm 7$ MPa; $\sigma_m = 974 \pm 11$ MPa; A%= 11 ± 0.3.

2.2. Fatigue test

Since the fatigue limit of the component was unknown and difficult to estimate a priori, the primary goal of the work was to obtain a life curve that could cover the finite life region and provide a first estimate of the loads corresponding to infinite life. Full scale fatigue tests were therefore carried out in room temperature on the conrods using Instron

Fig. 1. Lightweighted Ti6Al4V SLM conrod used in the present research (dimensions in mm).

multiaxial fatigue testing machine with a load cell capacity of 250kN in axial loading. Constant amplitude sinusoidal axial load cycles were applied to the conrod parts under tension and compression within different load ranges. The target life was set to 2×10^6 cycles and a total of seven tests with different values of maximum and minimum load were completed, while keeping fixed the load ratio of $R = -2.66$ and the loading frequency of 10 Hz. The chosen starting loads and loading ratio was assumed based on calculations carried out in a previous work [12], in which design criteria were developed starting from the modelling of the entire system (composed of crankshaft, engine piston and conrod) kinematics and considering real data for conrod length, rotational speed of engine and piston mass. Regarding loads applied for the first test, the peak loads were set to 29 kN in tension and −77 kN in compression. In general, these values depend on specific target application: maximum tension is related to the highest axial acceleration when the piston is in the top dead centre position and rotational speed is at the highest level, whereas maximum compression is instead related to the loading at maximum gas. For further details, see also the loadcase calculation reported in [12].

The test configuration shown in Fig. 2 was used for axial fatigue testing of conrod specimens. Using this testing setup, the specimens were loaded using two pins (located with red arrows in Fig. 2). The surfaces of the loading pins are in contact with the conrod in correspondence of the bearing holes; these areas were continuously lubricated during the course of fatigue loading. The lubrication was performed using a peristaltic pump with 1 bar oil pressure at the crank end bearing and drip lubrication at the piston pin end. In particular, the conrod was designed with conformed cooling channels integrated into the branches of its structure throughout the entire section from the small end to the big end of the part. This allows a more efficient lubrification than the machined linear channel of the forged version.

2.3. FEA model

In order to correlate applied loads and the resulting stress field in the conrod, fatigue test conditions were replicated via finite element (FE) simulations to analyze the stress and strain distributions and identify critical regions where stress components of a test loading cycle should be calculated for a fatigue life analysis. The analysis was carried out via DS Simulia Abaqus 2020 with standard implicit solver and the dynamic effects were not included as the body forces in testing conditions are negligible. An elastic modulus of 123000 MPa and a Poisson coefficient of 0.34 were considered. No plastic behavior was introduced as the resulting testing stress distribution was much lower than the 900 MPa yield stress of this Ti alloy.

The geometry of the connecting rod was reduced to one fourth (Fig. 3) due to the presence of two symmetry planes for the testing conditions. Both the bushings were not included in the analyses since they have no structural relevance. Both the pins were modelled as rigid discrete surfaces with the same diameter of the holes since the precision grade is very high and very tight coupling tolerances are prescribed (zero-backlash condition).

The mesh consisted of roughly 160,000 s order tetrahedra (C3D10) with an average characteristic length lower than 0.8 mm, reaching over 800,000 degrees of freedom (DOF) total. While the big-end pin was completely blocked with all the DOF being constrained, the small-end pin was unconstrained along the connecting rod axis to allow movement in the loading direction. Accordingly, the piston load was applied on the small-end pin and ranges from the maximum value of 29 kN (tension) to the minimum value of −77 kN (compression), the same as prescribed in the first fatigue test. In the end, a preload of 16 kN was also considered for the bolted connection of the big-end, following the company prescription for the conventional conrod that served as basis for this AM-topology optimized version. A surface-to-surface contact formulation was applied to account for the interactions between pins and connecting rod ends and between the two halves of the big-end. While the pin-rod interaction was considered frictionless, a coefficient of friction of 0.5 was introduced for the contact between the two halves of the big-end.

2.4. Microstructural observation before and after the test

A microstructural characterisation was conducted on the component. Different zones machined out of conrod were analysed in order to investigate the potential dissimilarity due to the different thickness of the parts. After the test, the fracture area was analysed both at a fracture surface level and on sections closed to this zone to guarantee a complete overview of the component structural behaviour also from a metallurgical point of view. The surfaces were prepared with standard metallographic techniques (ground with SiC papers and polished with 1 μm diamond paste) and were etched with a 10 ml H_2O, 5 ml HNO_3 and 1 ml HF solution. The microstructure of the sections was examined using a Leica DMI 5000 M optical microscope. Fracture surface observations were conducted using Scanning Electron Microscopy (FEI, Quanta™ 650 FEG, Oregon, USA).

Fig. 2. Fatigue test configuration including the loading blocks, conrod specimen, and the oil tray.

Fig. 3. Connecting rod geometry as modelled for the finite element analyses. The full geometry was cut along the two symmetry planes. The gray surfaces are the discrete rigid surfaces of the pins.

3. Results and discussion

3.1. Fatigue test

The fatigue tests were performed under four different loading levels and the results in form of maximum load versus the number of cycles to failure are presented in Fig. 4. As stated before, the test with the highest applied load ($F_{max} = 29$kN and $F_{min} = -77$kN) was selected based on the realistic loading condition of the conrod part. In that case, a fatigue life of 58,488 was obtained which is lower than the conventional conrod fabricated via forging (10^7). As a reason for this observation, the higher surface roughness of AM component can be pointed out. By keeping the loading ratio constant and reducing the maximum applied load, the double logarithmic diagram in Fig. 4 was obtained. According to the statistical analysis on the fatigue data, a scatter index (the ratio between the load level corresponding to 10% and 90% of survival probability) of 1.497 was obtained which is slightly higher than the reported value of 1.328 for smooth SLM Ti6Al4V specimens in the literature [32]. The observed higher scatter can be linked to the lower number of tested specimens in the current research which results in higher scatter index. Besides, the mentioned smooth specimens were printed along the longitudinal axis of the specimen resulting in a more consistent surface roughness in the gauge length. While in conrod samples, in almost all cases, the failure occurred in the notch region of the conrod between the main axis and the crank end bearing where the free surface (i.e. fatigue initiation location) is an inclined surface with respect to the printing direction. Although the tested conrod is a relatively large component compared to the common fatigue test specimens, the obtained inverse slope of the fatigue data in Fig. 4 ($k = 5.53$) is close to the reported value for small coupons of the same alloy tested under $R = 0.01$ loading ratio ($k = 4.74$) [32]. Further studies are required to link the fatigue loading ratio and the obtained inverse slope of AM Ti6Al4V in presence of the surface roughness. The detailed description of the fatigue tests is provided in Table 1.

3.2. Stress fields from FEA

For better visual clarity, macroscopic contour maps are shown on the full conrod by mirroring results along the two symmetry planes.

Fig. 5 and Fig. 6 show the stress distribution for maximum tension and maximum compression respectively: for both figures the Von Mises, the maximum principal and the minimum principal stress maps are reported.

Both the maximum compression and the maximum tension loading conditions show comparable high stress regions near the bolt head due to the 16kN preload. When neglecting the bolt head region, the Mises stress peak is above 350 MPa for the tension load case and roughly 490

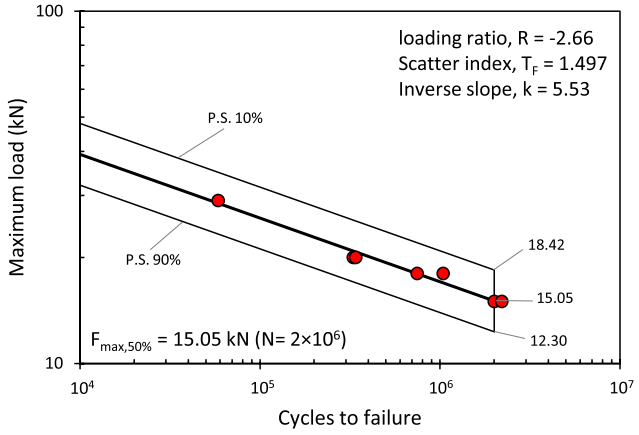

Fig. 4. Fatigue diagram of the tested specimens.

Table 1
Detail of fatigue tests on AM conrod specimens.

No	Maximum load (kN)	Minimum load (kN)	Loading ratio	Cycles to failure	Note
1	29	−77	−2.66	58,488	
2	20	−53.1	−2.66	329,038	
3	20	−53.1	−2.66	339,815	
4	18	−47.8	−2.66	745,235	
5	18	−47.8	−2.66	1,039,429	
6	15	−39.8	−2.66	2,000,000	Run-out
7	15	−39.8	−2.66	2,000,000	Run-out

MPa for the compression load case and, as expected, lower absolute stresses can be appreciated for the maximum tension loading condition due to a much lower absolute load value (+29 kN versus −77 kN). The stress distribution is mainly compressive for the compression load case and mainly tensional for the tension load case, but in the central region, where the complex shape of the conrod was designed according to topological optimization, the presence of some stress concentration at the connections between intersecting struts can be noticed, due to high curvatures. It should also be noted that the tensile and compressive loading conditions differ significantly in terms of stress distribution. Stress concentration regions move from the center of the connecting rod to the outer zones when switching from the compressive load to the tensioning load due to interaction with the pins and how this affects the stress flow. For the compressive condition, the load is transferred along the inner half of the connecting rod ends while for the tensioning condition, the load is transferred along the outer half of the connecting rod ends (for an easier understanding, see Fig. 7 for the contact pressure distribution).

As a consequence, some potentially critical locations could be identified by the FEM analysis in the outer struts that connect the central region to the big end and the notch at the connection between the big end and the central region. A detail of this region is shown in Fig. 8, including for each location, the principal stress values of three nodes along the thickness for both the maximum tension and compression conditions. Overall, these locations showed a mostly uniaxial stress state during the whole fatigue cycle, with the strut notch (location C) showing the least uniaxial condition. Specifically, when considering the + 29/−77 kN load case, the notch connecting the central region with the big-end (location A) shows a maximum principal stress of 390 MPa when loaded in tension and minimum principal stress of −214 MPa when loaded in compression, leading to a stress amplitude of 604 MPa and mean stress of 88 MPa. The strut body (location B), shows instead a lower maximum principal stress at 328 MPa when loaded in tension and a −413 MPa minimum principal stress when loaded in compression, corresponding to a 741 MPa stress amplitude and −43 MPa mean stress. In the end, the strut notch (location C) shows opposite stress signs (reversed-phase stress cycle) with a maximum principal stress of 455 MPa when loaded in compression and minimum principal stress of −200 MPa when loaded in tension, resulting in a 655 MPa stress amplitude and a 127 MPa mean stress.

Moreover, it could be noted that, due to how load transfers across the conrod geometry, the application of $R = -2.66$ loading ratio does not result in the same stress ratio at the critical locations identified on the model leading to $R = -0.55$ at the central notch (A), $R = -1.26$ on the outer struts body (B), and $R = -0.44$ at the notch of the outer strut (C).

While the stress values observed in this critical region are well below the static strength of the material, the comparison with fatigue strength data for life prediction is certainly less favorable. Unfortunately, these data are not yet available for the material under investigation and a comparison with the extensive literature on fatigue of additively manufactured titanium alloys is not straightforward, because of the huge number of variables involved, from processing parameters to post-

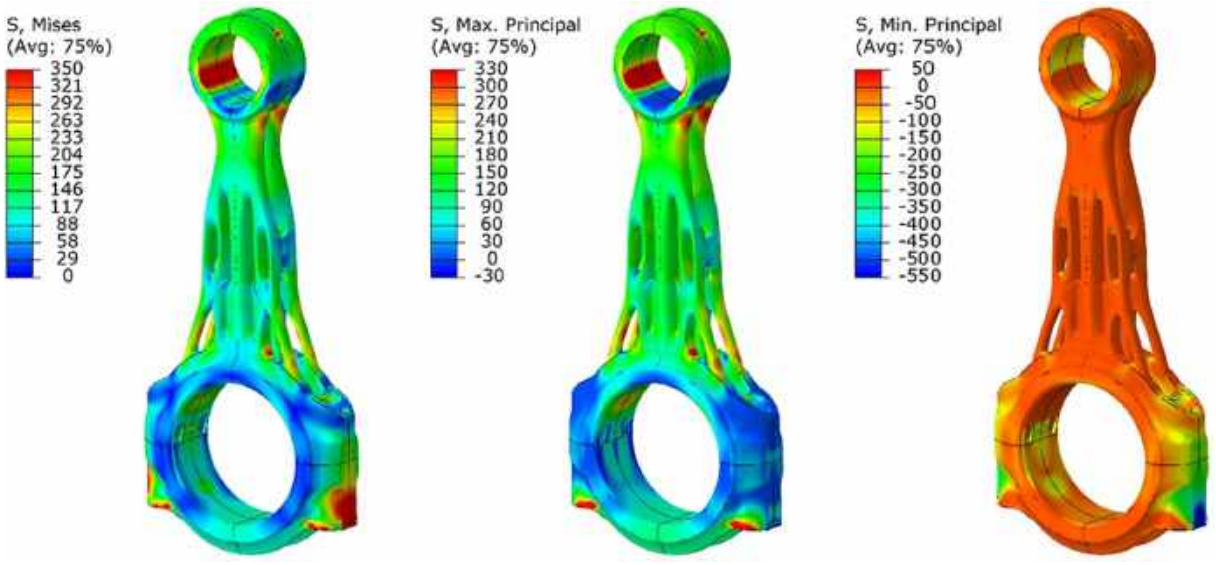

Fig. 5. Stress distributions for the maximum tension (+29kN load). From left to right: Von Mises, maximum principal and minimum principal stress maps; all values in MPa.

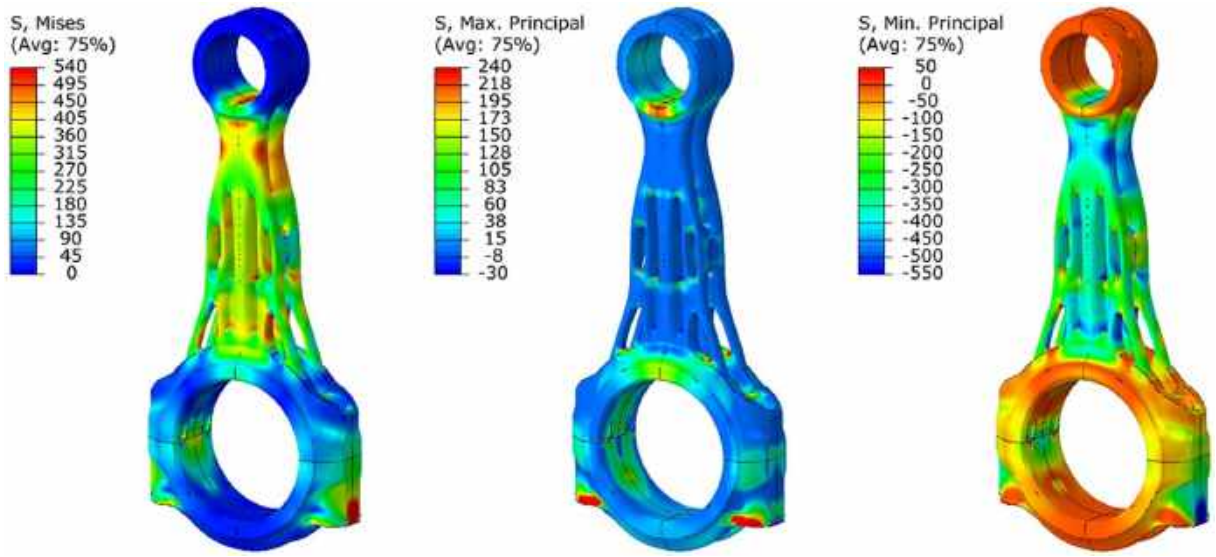

Fig. 6. Stress distributions for the maximum compression (-77kN load). From left to right: Von Mises, maximum principal and minimum principal stress maps; all values in MPa.

processing strategies or loading conditions. Nevertheless, the results of FEA and experimental test clearly suggest that the design strategy for the conrod would benefit from the inclusion in the optimization process of some fatigue evaluation step. While this necessarily requires an extensive test campaign on the material, under the specific condition of interest, the results of the present work are a fundamental first step that may help to identify the best strategy to map results obtained at a specimen level to the component scale.

3.3. Analysis of fatigue fracture surfaces

Fig. 9 illustrates the representative failure location and the corresponding fracture surface of the tested conrod specimens under fatigue loading. As can be seen from Fig. 9, the fatigue failure initiation location is consistent with the finite element results. In this scenario, the fatigue failure has started at the location of maximum principal stress when the conrod is loaded under tension (see Fig. 8). The stress value in this area is one of the highest foreseen in the entire part, but it is well below the static strength of the material and it couldn't be compared with reference fatigue values due to the high scatter of literature on this topic as already mentioned in the introduction. So it can be deduced that the early crack initiation in the part resulted from the interaction of the high stress concentration in this area together with the presence of surface defects induced by the SLM process that led to a stress intensification in this region.

While the remelting of the scanned sections during SLM process can improve the quality of the fabricated parts and possibly reduce the pores in the material, some limited areas on the upward faces of the fabricated do not experience such remelting on the last track, increasing the possibility of presence of remaining defects in these areas. In the tested conrod specimens, the maximum depth of the surface defects was in a range between 130 and 200 μm. In presence of a fatigue crack in this area, the displacement range would eventually increase and result in failure of the connecting beams in the part. According to the optical and

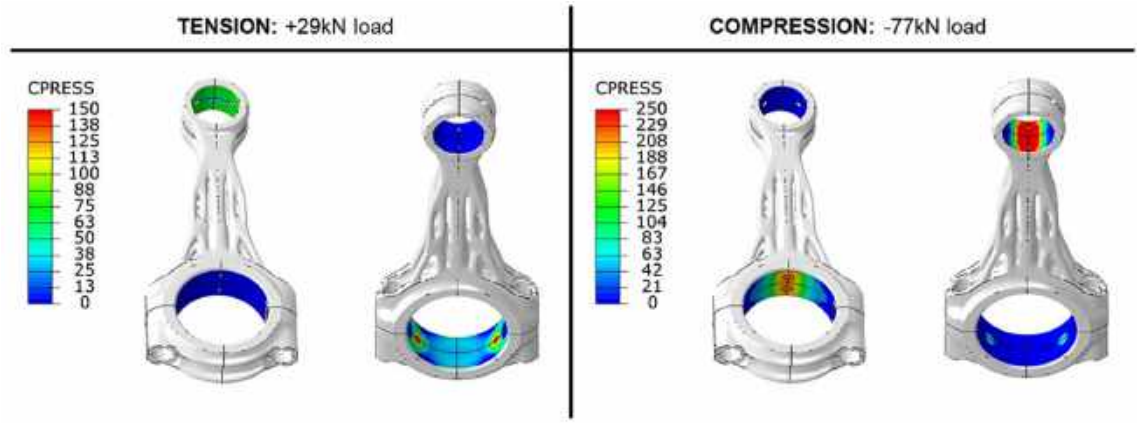

Fig. 7. Contact Pressure (CPRESS) distributions for the maximum tension and compression loads; all values in MPa.

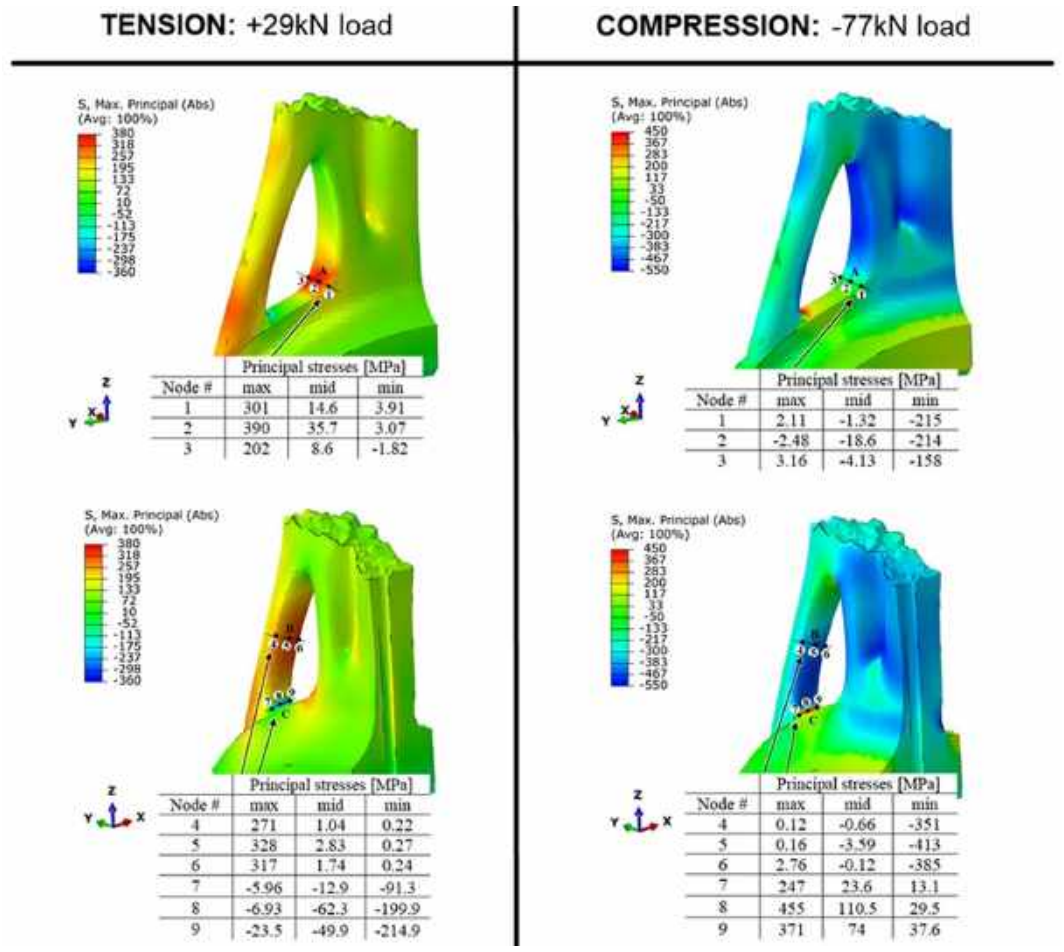

Fig. 8. Detail contour map of maximum absolute principal stress at critical locations for maximum tension and maximum compression conditions. Nodes 1, 2 and 3 show principal stress components at the central notch location (A) while nodes 4, 5 and 6 refer to the strut body location (B) and 7, 8 and 9 refer to the strut notch location (C).

scanning electron microscopy results, two initiation points can be detected on the fracture surface verifying the fact of parallel fatigue crack growth on both sides of the conrod part through the thickness. The general pattern of fatigue failure in the specimens represents a brittle type of failure including transgranular type of failure on the fracture surface with preferable plane orientation with regard to the crystallographic orientation of the materials grains. These failure features lack the typical ductile dimples also in the final rupture area which is commonly observed for wrought Ti-6Al-4 V material [31]. Evaluation of the fracture surface revealed no presence of any type of internal defect in the fabricated part verifying the high printing quality of the bulk material. It is worth mentioning that the detailed inspection of the fracture surface around the lubrication channels confirmed the lack of fatigue crack initiation in these locations.

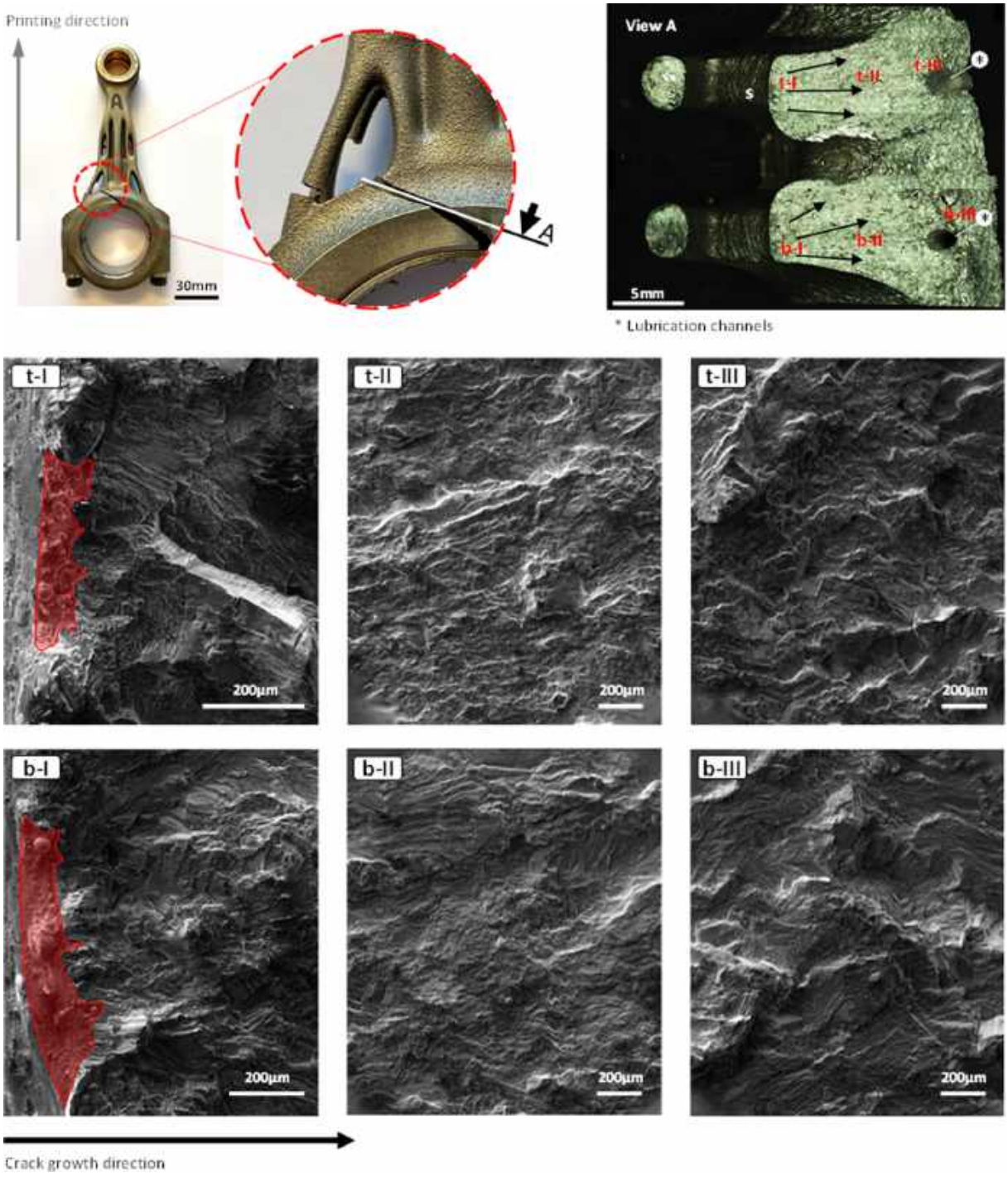

Fig. 9. Representative optical microscopy and SEM analysis of the fracture area in the tested conrod specimen under a maximum load of Fmax = 18kN.

3.4. Microstructural observation before and after the test

Fig. 10 shows an example of the microstructure analysed on samples cut of from the SLM conrods before the test. Note that during optical microscope analysis the α phase appears light and the β phase dark.

The macrostructure (lower magnifications Fig. 10 a,b) is composed of equiaxial previous β grains, obtained after the heat treatment above the β transus temperature. Indeed, this kind of heat treatment was specifically selected in order to enable the transformation of the original β grains, anisotropically oriented through the building direction, into new equiaxial grains.

From a microstructural point of view (higher magnifications Fig. 10 c,d), inside the previous β grains thin α and β lamellae can be observed; in addition at previous β grain boundaries an almost continuous α layer can be observed, as clear from the details reported in Fig. 10 d.

After the tests, the microstructure observed along the conrod was overall comparable to the one observed in Fig. 10. Anyway, few defects were observed in some limited areas of the component surface as highlighted in Fig. 11. These details are magnifications of some zones not far from the fracture surface (red rectangle) and it is worthwhile to note that they are localized in restricted zones alternately with an overall sound surface. The defects observed were unmelted powder (Fig. 11 b arrow 1) and pores (Fig. 11 b arrow 2). Then, Fig. 11 c,d show an example of growth of α lamellae size, that was observed in limited areas having an average thickness of 81 ± 24 µm. As is known, even though they are limited in amount, these defects could affect the fatigue

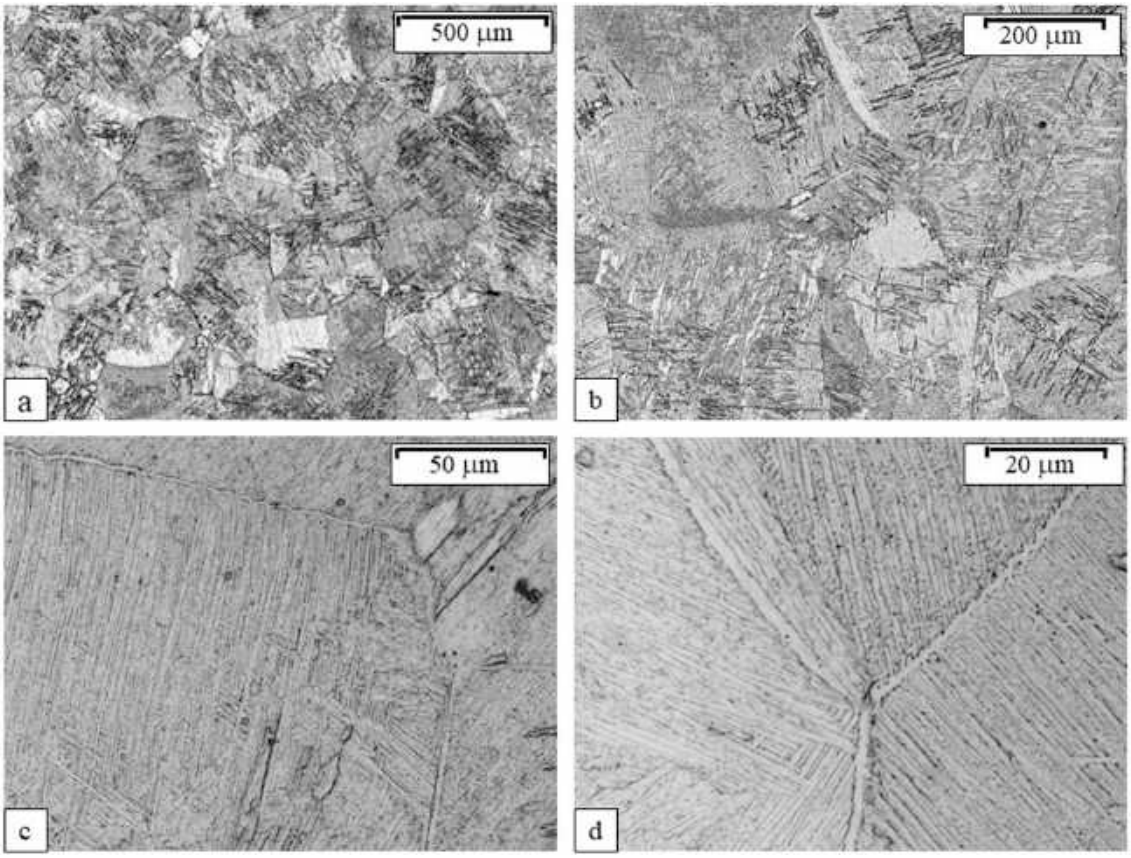

Fig. 10. Microstructure of SLM Ti6Al4V conrod sections at different magnifications.

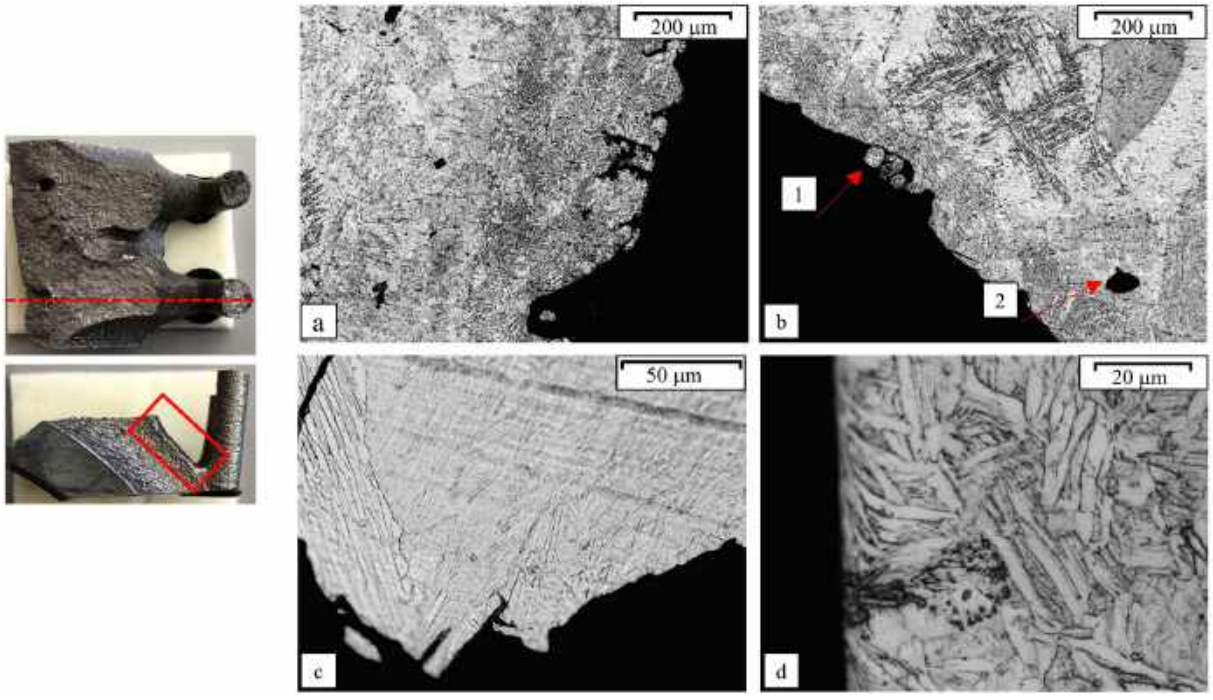

Fig. 11. Focus on defects near the fracture surface of SLM Ti6Al4V conrod sections at different magnifications.

performance of the component acting as early crack initiation [39]. Thus, a future extension of the present work should address a further reduction of these defects that can be reached for example with specific post-treatments and contouring strategies.

Fig. 12 shows a transversal section of the fracture surface at different magnifications. In order to better explain the following comments, please note that in the images red arrows located cracks while black arrows located β Grain Boundary (GB). Low magnifications (Fig. 12 a,b)

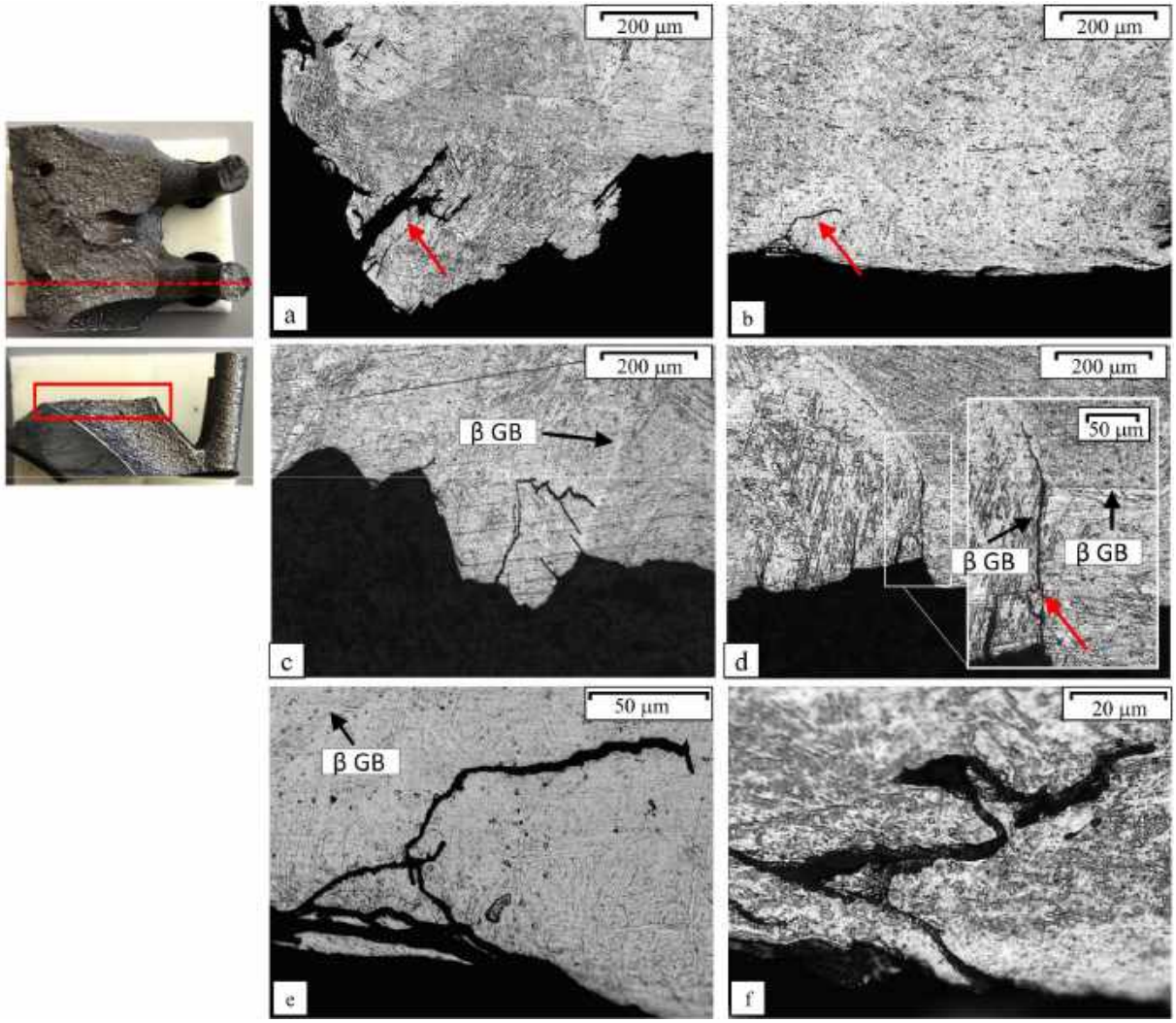

Fig. 12. Microstructure of the cross section of the fracture surface of SLM Ti6Al4V conrod sections at different magnifications.

revealed the presence of some secondary cracks branched through thickness direction, while higher magnifications (Fig. 12 c, e, f) clarify that their propagation is mainly transgranular, with frequent changes of path along the different α colonies. In particular, it was observed that the secondary cracks exhibited a greater tendency to modify their direction when they interact with coarser α lamellae regions; also the orientation of the α lath has an influence on the crack path, offering a favourable propagation when their directions are aligned. In addition, some few events of secondary cracks were observed along the first α phase that lies along previous β grain boundaries (see Fig. 12 d). Generally, this microstructure causes a zigzag crack front without evidence of crack branching.

4. Conclusions

Fatigue behaviour of topologically optimized Ti6Al4V connecting rods fabricated via selective laser melting was evaluated by performing stress analysis on the designed component and experimental testing of the fabricated parts under applied loads representative of operating service. The tested design was developed for weight reduction of motorsport engines and consisted of a non-conventional multi-branch structure. The microstructure of the bulk material included previous β grains composed of very fine α and β lamellae and α layer at their grain boundaries.

Based on the performed numerical and experimental analyses, the main results can be summarized as follows:

- A fatigue life diagram that covers the finite life region and provides a first estimate of the loads corresponding to infinite life ($F_{max,50\%}$=15.05 kN, N = $2*10^6$) was achieved. This was one of the research targets since the fatigue limit was unknown and difficult to estimate a priori.
- The combination of material defects, surface finish and presence of geometrical variations led to a significant reduction of the fatigue strength compared to the conventional conrod part. Indeed, the highest applied load (F_{max} = 29kN and F_{min} = -77kN) led to a lower fatigue life when compared with the conventional conrod fabricated via forging (58,488 vs 10^7 cycles). In this context, end of life analysis underlines that in a limited area on the upward a surface defect was identified located in the most loaded zone of the component.
- The fatigue failure initiation location was well in agreement with the results of the numerical analysis, emphasizing that the global geometrical discontinuity (i.e. notches generated by topology optimized design) was the governing factor in failure initiation. The fatigue failure initiated from the regions where the maximum principal stress was maximum under tensile load. The effects of higher stress levels in these areas were then amplified by the surface defect. Thus, the experimental and FEA results clearly suggest that the conrod design strategy could be improved by including some kind of fatigue evaluation step in the optimization process.

- From microstructural investigations, some secondary cracks with transgranular propagation were observed on the transversal section of the fracture surface; here it was detected a tendency of the crack to modify its direction when in contact with coarser α lamellae regions.

Considering the geometry and location dependent surface quality of the parts, test coupons with representative notch geometries and building orientation should be tested and used for calibration of local fatigue prediction criteria such as the theory of critical distances and strain energy density. Also, an additional post-process aimed at further reducing surface asperities and defects could be a possible improvement to be considered. While this necessarily requires an extensive test campaign of the material under specific conditions of interest, the results of the present work are a fundamental first step toward fatigue assessment of full-scale components fabricated with SLM and may help correlating results obtained at a specimen level to predictions at a component scale.

Declaration of Competing Interest

The authors declare that they have no known competing financial interests or personal relationships that could have appeared to influence the work reported in this paper.

Acknowledgements:

The authors are grateful: for the cooperation during the Design for Additive Manufacturing development to Additive Mind department from EOS GmbH; for the support in the machine tool design and manufacturing to Streparava Spa, particularly to ing. Matteo Magni and ing. Luca Cordioli; for the heat treatments execution to TAV vacuum furnaces SpA, particularly to ing. Alessandro Fiorese and ing. Andrea Gionda.

References

[1] Additive manufacturing - qualification and certification process for materials and components, accessed September 2020, https://rules.dnvgl.com/docs/pdf/DNVGL/CG/2017-11/DNVGL-CG-0197.pdf.
[2] Helms H, Lambrecht U. The potential contribution of light-weighting to reduce transport energy consumption. Int J Life Cycle Assess 2007;12:58–64.
[3] Cecchel S. Materials and technologies for lightweighting of structural parts for automotive applications: a review. SAE Int J Mater Manf 2021;14(1):81–97. https://doi.org/10.4271/05-14-01-0007.
[4] Cecchel S, Ferrario D, Panvini A, Cornacchia G. Lightweight of a cross beam for commercial vehicles: development, testing and validation. Mater Des 2018;149:122–34. https://doi.org/10.1016/j.matdes.2018.04.021.
[5] Cecchel S, Ferrario D, Mondini C, Montani M, Previtali B. Application of laser metal deposition for a new model of assembled camshaft. J Mater Eng Perform 2019;28:7756–67. https://doi.org/10.1007/s11665-019-04504-2.
[6] The potential for mass reduction of passenger cars and light commercial vehicles in relation to future CO_2 regulatory requirements: Appendices; https://ec.europa.eu/clima/sites/clima/files/transport/vehicles/docs/ldv_downweighting_co2_appendices_en.pdf.
[7] Sroka ZJ, Cieślak M. An impact of engine downsizing on change of engine weight. J kones 2019;22:213–9. https://doi.org/10.5604/12314005.1165440.
[8] Khurmi RS, Gupta JK. A textbook of machine design. S Chand Publishing 2005.
[9] Qiu JW, Liu Y, Liu YB, Liu B, Wang B, Earle Ryba HP, et al. Microstructures and mechanical properties of titanium alloy connecting rod made by powder forging process. Mater Des 2012;33:213–9. https://doi.org/10.1016/j.matdes.2011.07.034.
[10] Froes FH, Friedrich H, Kiese J, et al. Titanium in the family automobile: the cost challenge. JOM 2004;56:40–4. https://doi.org/10.1007/s11837-004-0144-0.
[11] Schauerte O. Titanium in automotive production. Adv Eng Mater 2003;6:411–8. https://doi.org/10.1002/adem.200310094.
[12] Cecchel S, Ferrario D, Mega F, Cornacchia G. Numerical, mechanical, and metallurgical investigation of an innovative near net shape titanium selective laser melting engine component and comparison with the conventional forged one. Adv Eng Mater 2021;23(7):2100036.
[13] Cecchel S, Ferrario D, Cornacchia G, Gelfi M. Development of heat treatments for Selective Laser Melting Ti6Al4V alloy: effect on microstructure, mechanical properties and corrosion resistance. Adv Eng Mater 2020;22(8):2000359.
[14] Afzal A, Fatemi A. A Comparative Study of Fatigue Behavior and Life Predictions of Forged Steel and PM Connecting Rods 2004. https://doi.org/10.4271/2004-01-1529.
[15] Romano S, Brandão A, Gumpinger J, Gschweitl M, Beretta S. Qualification of AM parts: extreme value statistics applied to tomographic measurements. Mater Des 2017;131:32–48. https://doi.org/10.1016/j.matdes.2017.05.091.
[16] Benedetti M, Fontanari V, Bandini M, Zanini F, Carmignato S. Low- and high-cycle fatigue resistance of Ti-6Al-4V ELI additively manufactured via selective laser melting: mean stress and defect sensitivity. Int J Fatigue 2018;107:96–109. https://doi.org/10.1016/j.ijfatigue.2017.10.021.
[17] Günther J, Krewerth D, Lippmann T, Leuders S, Tröster T, Weidner A, et al. Fatigue life of additively manufactured Ti–6Al–4V in the very high cycle fatigue regime. Int J Fatigue 2017;94:236–45.
[18] Chastand V, Tezenas A, Cadoret Y, Quaegebeur P, Maia W, Charkaluk E. Fatigue characterization of Titanium Ti-6Al-4V samples produced by additive manufacturing. Procedia Struct Integr 2016;2:3168–76. https://doi.org/10.1016/j.prostr.2016.06.395.
[19] Leuders S, Thöne M, Riemer A, Niendorf T, Tröster T, Richard HA, et al. On the mechanical behaviour of titanium alloy TiAl6V4 manufactured by selective laser melting: fatigue resistance and crack growth performance. Int J Fatigue 2013;48:300–7.
[20] Wycisk E, Emmelmann C, Siddique S, Walther F. High Cycle Fatigue (HCF) Performance of Ti-6Al-4V alloy processed by selective laser melting. Adv Mater Res 2013;816–817:134–9. https://doi.org/10.4028/www.scientific.net/AMR.816-817.134.
[21] H. Soyama, F.Takeo, Effect of various peening methods on the fatigue properties of Titanium alloy Ti6Al4V manufactured by direct metal laser sintering and electron beam melting. Materials (Basel) 2020;13. 10.3390/ma13102216.
[22] Kahlin M, Ansell H, Basu D, Kerwin A, Newton L, Smith B, et al. Improved fatigue strength of additively manufactured Ti6Al4V by surface post processing. Int J Fatigue 2020;134:105497. https://doi.org/10.1016/j.ijfatigue.2020.105497.
[23] Pintado CN, Dominguez J, Perinan A, Garcia MH, Lasagni F, Bernarding S, et al. Effect of surface treatment on the fatigue strength of additive manufactured Ti6Al4V alloy. Frattura ed Integrità Strutturale 2020;14(53):337–44. https://doi.org/10.3221/IGF-ESIS.53.26.
[24] Morettini G, Razavi N, Zucca G. Effects of build orientation on fatigue behavior of Ti-6Al-4V as-built specimens produced by direct metal laser sintering. Procedia Struct Integr 2019;24:349–59. https://doi.org/10.1016/j.prostr.2020.02.032.
[25] Edwards P, Conner AO, Ramulu M. Electron beam additive manufacturing of titanium components: properties and performance. J Manuf Sci Eng 2013;135(6):061016. https://doi.org/10.1115/1.4025773.
[26] Edwards P, Ramulu M. Fatigue performance evaluation of selective laser melted Ti–6Al–4V. Mater Sci Eng A 2014;598:327–37. https://doi.org/10.1016/j.msea.2014.01.041.
[27] Tan X, Kok Y, Tan YJ, Vastola G, Pei QX, Zhang G, et al. An experimental and simulation study on build thickness dependent microstructure for electron beam melted Ti-6Al-4V. J Alloys Compd 2015;646:303–9. https://doi.org/10.1016/j.jallcom.2015.05.178.
[28] X. Tan, Y. Kok, W.Q. Toh, Y.J. Tan, M. Descoins, D. Mangelinck, S.B. Tor, K.F. Leong, C.K. Chua Revealing martensitic transformation and α/β interface evolution in electron beam melting three-dimensional-printed Ti-6Al-4V, Sci. Rep., 6 (2016), pp. 1-10. 10.1038/srep26039.
[29] Razavi N, Van Hooreweder B, Berto F. Effect of build thickness and geometry on quasi-static and fatigue behavior of Ti-6Al-4V produced by electron beam melting. Addit Manuf 2020;36:101426. https://doi.org/10.1016/j.addma.2020.101426.
[30] Razavi N, Ferro P, Berto F. Fatigue assessment of Ti–6Al–4V circular notched specimens produced by selective laser melting. Metals (Basel) 2017;7:291. https://doi.org/10.3390/met7080291.
[31] Razavi N, Berto F. Directed energy deposition versus wrought Ti-6Al-4V: a comparison of microstructure, fatigue behavior, and notch sensitivity. Adv Eng Mater 2019;21(8):1900220. https://doi.org/10.1002/adem.201900220.
[32] Razavi N, Ferro P, Berto F, Torgersen J. Fatigue strength of blunt V-notched specimens produced by selective laser melting of Ti-6Al-4V. Theor Appl Fract Mech 2018;97:376–84. https://doi.org/10.1016/j.tafmec.2017.06.021.
[33] Waddell M, Walker K, Bandyopadhyay R, Kapoor K, Mallory A, Xiao X, et al. Small fatigue crack growth behavior of Ti-6Al-4V produced via selective laser melting: in situ characterization of a 3D crack tip interactions with defects. Int J Fatigue 2020;137. https://doi.org/10.1016/j.ijfatigue.2020.105638.
[34] Ferreira FF, Neto DM, Jesus JS, Prates PA, Antunes FV. Numerical prediction of the fatigue crack growth rate in SLM Ti-6Al-4V based on crack tip plastic strain. Metals 2020;10(9):1133. https://doi.org/10.3390/met10091133.
[35] Yadollahi A, Shamsaei N. Additive manufacturing of fatigue resistant materials: challenges and opportunities. Int J Fatigue 2017;98:14–31. https://doi.org/10.1016/j.ijfatigue.2017.01.001.
[36] Li P, Warner D, Fatemi A, Phan N. Critical assessment of the fatigue performance of additively manufactured Ti–6Al–4V and perspective for future research. Int J Fatigue 2016. https://doi.org/10.1016/j.ijfatigue.2015.12.003.
[37] Chern AH, Nandwana P, Yuan T, Kirka MM, Dehoff RR, Liaw PK, et al. Int J Fatigue 2019;119:173–84. https://doi.org/10.1016/j.ijfatigue.2018.09.022.
[38] Fatemi A, Molaei R, Simsiriwong J, Sanaei N, Pegues J, Torries B, et al. Fatigue behaviour of additive manufactured materials: An overview of some recent experimental studies on Ti-6Al-4V considering various processing and loading direction effects. Fatigue Fract Eng Mater Struct 2019;42(5):991–1009. https://doi.org/10.1111/ffe.13000.
[39] Shamir M, Khadar Syed A, Janik V, Biswal R, Zhang X. The role of microstructure and local crystallographic orientation near porosity defects on the high cycle fatigue life of an additive manufactured Ti-6Al-4V. Mater Charact 2020;169:110576. https://doi.org/10.1016/j.matchar.2020.110576.